Ab Initio Study of Cyclobutane: Molecular Structure, Ring-Puckering Potential, and Origin of the Inversion Barrier

Eric D. Glendening* and Arthur M. Halpern

Department of Chemistry, Indiana State University, Terre Haute, Indiana 47809

Received: July 26, 2004

The structure and ring-puckering properties of cyclobutane and its perdeuterated isotopomer are studied using high-level ab initio methods and complete basis set extrapolations. Calculations reveal significant coupling between the ring-puckering (θ) and CH_2-rocking (α) motions, with equilibrium angles ($\theta_{eq} = 29.59°$ and $\alpha_{eq} = 5.67°$) that are within the range of experimentally determined values. Our best estimate of the inversion barrier is 482 cm^{-1}, in excellent agreement with recent experimental determinations. Ring-inversion transition frequencies are evaluated from the eigenstates of the intrinsic reaction coordinate potentials for cyclobutane and cyclobutane-d_8. Natural bond orbital analysis shows that $\sigma_{CC} \rightarrow \sigma_{CH}^*$ and $\sigma_{CH} \rightarrow \sigma_{CH}^*$ hyperconjugative interactions are strengthened as cyclobutane puckers, thereby suggesting that inversion barriers in four-membered ring systems are a consequence of electronic delocalization rather than torsional strain.

Introduction

About 60 years ago, Rathjens et al. deduced on the basis of heat capacity and infrared (IR) spectroscopic measurements that ring-puckering motion in cyclobutane connected two equivalent equilibrium bent structures (D_{2d}), separated by a low-energy barrier associated with the planar (D_{4h}) form.[1,2] Furthermore, Rathjens et al. analyzed the IR data in terms of a double minimum potential consisting of quadratic wings and a Gaussian-shaped barrier having a height of ca. 370 cm^{-1}. The ring-puckering dihedral angle, θ, implicit in this potential is ca. 16°.[2] The motion connecting the two equivalent D_{2d} structures can be represented as the oscillation of two diagonal pairs of CH_2 groups along the C_4 symmetry axis that passes through the D_{4h} structure. Because of the low barrier associated with this process, not only is inversion a relatively fast process, but heavy-atom tunneling becomes a measurable characteristic of the system.

Many experimental and computational studies have addressed the molecular structure of cyclobutane and the nature of the ring-puckering potential.[3−24] In 1968, Ueda and Shimanouchi[3] analyzed CH_2 symmetric-stretch/ring-puckering combination bands in the IR spectrum in terms of a one-dimensional potential having quartic wings and an inverted quadratic barrier. On the basis of this analysis, they reported a barrier of 448 cm^{-1} and an equilibrium ring dihedral angle, θ_{eq}, of 34°. Wright and Salem[4] reported that ab initio calculations produced a double minimum potential only when CH_2 rocking is incorporated with ring puckering. Thus, the rigid bender model, in which the CH_2 rocking angle, α, defined as the angle between the ∠H−C−H bisector and the bisector of the corresponding ∠C−C−C angle (see Figure 1), is held fixed in the symmetrical position throughout the puckering motion (i.e., $\alpha = 0$), produced a single minimum potential. This work established the theoretical importance of coupling between the methylene rocking and ring-puckering motions.

Meiboom and Snyder[7] reported the 60 MHz proton NMR spectrum of cyclobutane in a nematic solvent at 80 °C, determining that under these conditions the molecule was either planar or in rapid interconversion between the two equivalent D_{2d} structures. Assuming the latter, Meiboom and Snyder were able to deduce models of the puckered-ring geometry on the basis of certain relationships between the NMR coupling constants and by assuming a C−C bond length. Their assignments of θ_{eq} and α_{eq} were 27 and 4° or 23 and 7°, respectively, depending on the structural model used. In the former case, they assumed equal equatorial and axial C−H bond lengths; and in the latter, they took the axial C−H bond length to be longer than the equatorial by 0.04 Å.

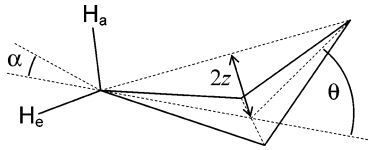

Figure 1. Definitions of the structural parameters θ, α, and z for D_{2d} cyclobutane.

Subsequent IR and Raman studies of cyclobutane have been carried out in which various workers have attempted to assign both the ring-puckering barrier, V_0, along with θ_{eq}. Several of these studies will be addressed later in this work, but we point out here that the nature of the spectroscopic analyses imposes certain constraints on the results. One stems from the limitation of using a strictly one-dimensional potential, usually expressed in terms of the distance between the midpoints of the lines connecting the pairs of diagonal C atoms, 2z, as shown in Figure 1. Another results from making certain structural dynamic assumptions about the puckering motion. For example, in the rigid bender model, it is assumed that α is zero for all values of z. In the semirigid bending model, coupling between CH_2 rocking and ring puckering is accounted for by assuming that α varies linearly with θ. These approaches, when used to determine the ring-puckering potential (hence V_0 and θ_{eq}) from spectroscopic data, require different expressions for the value of the reduced mass, μ, of cyclobutane or cyclobutane-d_8. For example, in applying the rigid bender model, Stone and Mills[6] use a constant value of μ of 106.6 amu (a value in fact larger

* Corresponding author. E-mail: glendening@indstate.edu.

10.1021/jp0405097 CCC: $30.25
Published on Web 01/05/2005

TABLE 1: Summary of Experimental Assignments of θ_{eq}, α_{eq}, δ_{eq}, and V_0

θ_{eq}	α_{eq}	δ_{eq}	V_0/cm^{-1}	method	ref
15.9			371	IR/Raman	*a*
33.4			448.1	IR	*b*
35			503	IR/Raman	*c*
22.8/27.0	6.75/3.85	0.142/0.297		NMR	*d*
35			518	IR/Raman	*e*
29-37	<7.5		514−516	reevaluation of IR/Raman	*f*
27.9−28.8	6.2	0.22	510	electron diffraction/IR	*g*
27.8	6.1	0.22	449	IR−2-d potential	*h*
28.6	5.3	0.18		microwave of C_4H_7D	*i*
29.55	5.7	0.19	504.7	microwave of $C_4H_6D_2$	*j*
31				X-ray diffraction	*k*

[a] Ref 2. [b] Ref 3. [c] Ref 6. [d] Ref 7. The listed values are based on $C-H_a = C-H_e$ and $C-H_a = C-H_e + 0.04$ Å, respectively. [e] Ref 8. [f] Ref 10. [g] Ref 16. [h] Ref 17. [i] Ref 18. [j] Ref 19. [k] Ref 22.

than the 56.06 amu mass of cyclobutane), while Malloy and Lafferty[10] employ a ring deformation coordinate-dependent reduced mass. In their analysis of the IR spectrum of the CH_2-rocking mode, Egawa et al.[17] account for higher order coupling between ring deformation and CH_2 rocking motions by applying a two-dimensional potential in terms of θ and α. From the various IR- or Raman-based studies, values of θ_{eq} have ranged between ca. 29 to 37°. Table 1 provides a summary of the experimental values of structural parameters and barrier heights.

Considering the lack of definitive information about the detailed molecular structure of cyclobutane, particularly θ_{eq}, and the interrelationship between V_0, θ_{eq} and α_{eq}, we carried out high-level ab initio calculations of the molecular geometries of the D_{2d} and D_{4h} structures. In addition, we obtained intrinsic reaction coordinate (IRC)[25,26] potentials for the ring-puckering motion in cyclobutane and cyclobutane-d_8 and examined the quality of these surfaces by comparing the calculated transition frequencies with experimental results. Given the clear need to account for ring puckering in terms of the coupling between θ, α, and perhaps other degrees of freedom, we were interested to determine the extent to which these essentially one-dimensional IRC potentials are able to capture the energetic properties and predict spectroscopic transitions associated with ring-puckering motion in cyclobutane. Furthermore, anticipating the heavy CH_2-CH_2 masses tunneling through this relatively low energy barrier, we sought to obtain reliable estimates of the tunneling frequencies of the ground and lower excited ring-inversion states.

It has long been recognized that the equilibrium ring geometry in cyclobutane reflects the interplay between the relief of ring strain, favoring a planar structure, and the minimization of torsional strain, which promotes a puckered geometry. Understanding the nature and energetics of four-membered ring systems is of fundamental importance in small ring chemistry and has particular implications in such important classes of compounds as thymine dimers and β-lactams. We also present in this paper a quantitative evaluation of the mechanism of the inversion barrier in cyclobutane using natural bond orbital (NBO) analysis.[27,28] Our calculations suggest that the inversion barrier can be best understood in terms of the loss of hyperconjugative stabilization in the planar geometry.

Calculations

Geometry optimizations were performed using density functional theory (specifically, the B3LYP hybrid functional),[29] second-order Moller−Plesset perturbation theory (MP2),[30] and the coupled cluster method with single and double excitations and perturbative triples [CCSD(T)].[31] Dunning's correlation consistent basis sets, cc-pVXZ (X = D, T, Q),[32] were used for all atoms. Calculations were completed with either GAMESS,[33] MOLPRO,[34] or Gaussian 98.[35]

Intrinsic reaction coordinate (IRC) calculations at the MP2/cc-pVTZ level were carried out using GAMESS with the Gonzalez−Schlegel[36] second-order algorithm. A step size of 0.1 or 0.2 bohr-amu$^{1/2}$ was used, depending on the IRC region. The central portion of the IRC, corresponding to the relaxation from the planar D_{4h} to the equilibrium D_{2d} structure, was obtained starting with the fully optimized planar form (IRC = 0). A total of 35 points was obtained along the IRC surface for cyclobutane, converging to within 0.07 cm^{-1} of the fully optimized D_{2d} energy. The out-lying or wing portion of the potential was acquired by performing a separate IRC scan starting from a partially optimized D_{2d} structure in which θ was constrained to a value of about 58°. The wing IRC consisted of 13 points and converged to within 0.72 cm^{-1} of the equilibrium D_{2d} energy. The two IRC scans were pieced together and then reflected with respect to IRC = 0 to represent the full, double minimum potential surface. The same procedure was used to obtain the potential for cyclobutane-d_8, except that the mass of D (2.014 amu) replaced that of H. Note that Cartesian d and f functions were used in all GAMESS calculations rather than the standard spherical harmonic functions of the correlation consistent basis sets.

Coupled cluster energy evaluations were performed with MOLPRO at all points along the IRC pathway. For each point, the CCSD(T) energy, $E(X)$, was extrapolated to the complete basis set (CBS) limit using the correlation consistent basis sets and the mixed exponential plus Gaussian fitting function[37,38]

$$E(X) = E_{CBS} + A \exp[-(X-1)] + B \exp[-(X-1)^2] \quad (1)$$

where A, B, and E_{CBS} are fitting parameters, E_{CBS} is the estimated energy in the CBS limit, and X is the cardinal number of the basis set (X = 2, 3, 4 for double-, triple- and quadruple-ζ sets, respectively). CCSD(T)/CBS-corrected IRC potentials were diagonalized using a finite element method to obtain the inversion eigenstates.

NBO analysis[28] of the hyperconjugative interactions was performed using Gaussian 98.

Molecular Structure and Inversion Barrier

The detailed structure of cyclobutane has not been obtained unambiguously from spectroscopic studies. In particular, the ability to deduce the degree of ring puckering (i.e., θ_{eq}) from vibrational spectroscopy depends significantly on the model selected to account for coupling between the ring-puckering (θ) and CH_2-rocking (α) motions. Table 1 summarizes the experimental studies of the cyclobutane structure. Estimates of θ_{eq} range from ca. 16 to 35°, although the more recent studies have rather consistently yielded values between 28 and 30°. Estimates of α_{eq} range from 5 to 7.5°. For example, based on a combination of gas-phase electron diffraction data and infrared spectra, Egawa et al.[16] assigned values of θ_{eq} and α_{eq} of 27.9 and 6.2°, respectively.

In view of the apparent uncertainty in the experimentally determined values of θ and α, one of the objectives of this study is to obtain these quantities, as well as other structural features of cyclobutane, using high-level ab initio calculations. We carried out full optimizations of D_{2d} cyclobutane using the

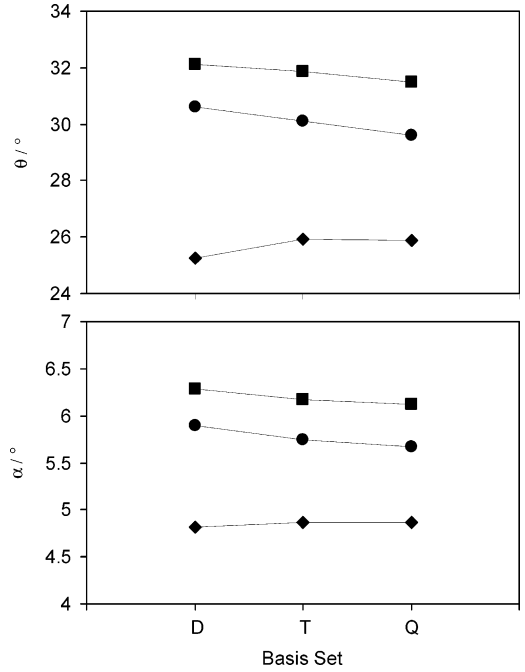

Figure 2. Basis set dependence of the equilibrium θ and α parameters for D_{2d} cyclobutane. The levels of theory employed are B3LYP (diamonds), MP2 (squares), and CCSD(T) (circles) with the cc-pV*X*Z basis sets.

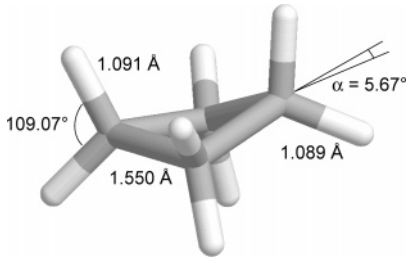

Figure 3. D_{2d} cyclobutane at the CCSD(T)/cc-pVQZ optimized geometry, showing the alternating pattern of axial and equatorial C−H bonds. Additional optimized parameters include ∠C−C−C = 88.07° and θ = 29.59°.

B3LYP, MP2, and CCSD(T) methods with the series of basis sets cc-pV*X*Z (*X* = D, T, Q). Optimizations of the D_{4h} geometry were also performed because of our interest in the inversion barrier. These calculations generally revealed that structural parameters are nearly independent of the basis set selected and depend only weakly on the level of theory. For example, Figure 2 shows the method and basis set dependence of the θ and α parameters for D_{2d} cyclobutane. At the CCSD(T)/cc-pVQZ level, θ_{eq} is 29.6°, in excellent agreement with the experimental estimates of Table 1. B3LYP calculations yield smaller torsion angles near 26° whereas MP2 gives larger angles of approximately 32°. Figure 3 shows the D_{2d} structure of cyclobutane optimized at the highest level of theory employed here, namely, CCSD(T)/cc-pVQZ. The optimized parameters for D_{4h} cyclobutane at this level are C−C = 1.554 Å, C−H = 1.089 Å, and ∠H−C−H = 108.26°.

Experimental estimates of the inversion barrier, V_0, in Table 1 range from 371 to 518 cm^{-1}, with most recent work generally yielding values between 500 and 520 cm^{-1}. Figure 4 shows computational estimates of the barrier height. Importantly, we find that V_0 depends rather strongly on the method and basis set selected. For example, CCSD(T) gives barriers of 664, 641, and 546 cm^{-1} for the double-, triple-, and quadruple-ζ basis sets, respectively. Extrapolating the CCSD(T) energies to the CBS limit yields a barrier of 482 cm^{-1}, which is in particularly good agreement with recent experimental estimates. Similar extrapolations, however, of the B3LYP and MP2 potentials give values of 676 and 300 cm^{-1} that compare considerably less favorably with experiment. However, we note that the barrier results are not strongly influenced by the method and basis set selected for the geometry optimization of cyclobutane. For instance, CCSD(T)/CBS barriers calculated at the MP2, B3LYP, and CCSD(T) geometries, each optimized with the cc-pVTZ basis set, are 464, 457, and 481 cm^{-1}, respectively. These results suggest that it is not particularly important which method and basis set are chosen for geometry optimizations of cyclobutane but that the ring-puckering potential should be evaluated using a highly correlated method with basis set extrapolation.

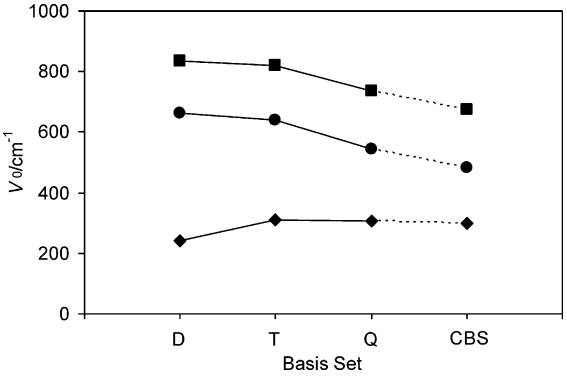

Figure 4. Basis set dependence of the inversion barrier, V_0, for cyclobutane and estimates of V_0 in the CBS limit. The levels of theory employed are B3LYP (diamonds), MP2 (squares), and CCSD(T) (circles) with the cc-pV*X*Z basis sets.

Ring-Puckering Potentials

The IRC potential represents the minimum energy pathway followed by the cyclobutane molecule as it undergoes large amplitude motion in which the ring flexes from the D_{4h} transition state through the equilibrium D_{2d} structures and into the wing regions defined by highly strained puckered geometries. These potentials are depicted in Figure 5 in which it can be seen that, consistent with deuterium substitution, the cyclobutane-d_8 potential extends out to larger IRC values than for cyclobutane. Accordingly, the minima of these potentials are at ±2.19 Å-amu$^{1/2}$ and ±1.67 Å-amu$^{1/2}$, respectively. Figure 5 also indicates the lowest four eigenvalue sets associated with inversion in cyclobutane and cyclobutane-d_8. These results will be discussed in connection with the relevant spectroscopic data for the following compounds.

It is evident in Table 1 that the ratio of the equilibrium CH_2 rocking angle to the dihedral angle (i.e., δ_{eq}), obtained from several different spectroscopic and structural studies, is nearly constant, lying between 0.18 and 0.22. The value of δ represents the degree of coupling between CH_2 rocking and ring puckering and is a key feature in modeling the inversion potential. Our computational results indicate that δ_{eq} is within this range and is nearly method and basis set independent. Thus, from the nine calculations represented in Figure 2, δ_{eq} = 0.192 ± 0.003. To examine the degree of this coupling for structures beyond the equilibrium state, we obtained values of δ for a number of geometries along the IRC. These results are shown in Figure 6 in which α is plotted versus θ. It appears that for values of θ up to about 45°, the slope of this plot (i.e., δ) is nearly constant, with a value of 0.185 (cf δ_{eq} = 0.192). This behavior is consistent with the semirigid bender model that has been used to analyze inversion in cyclobutane.[23]

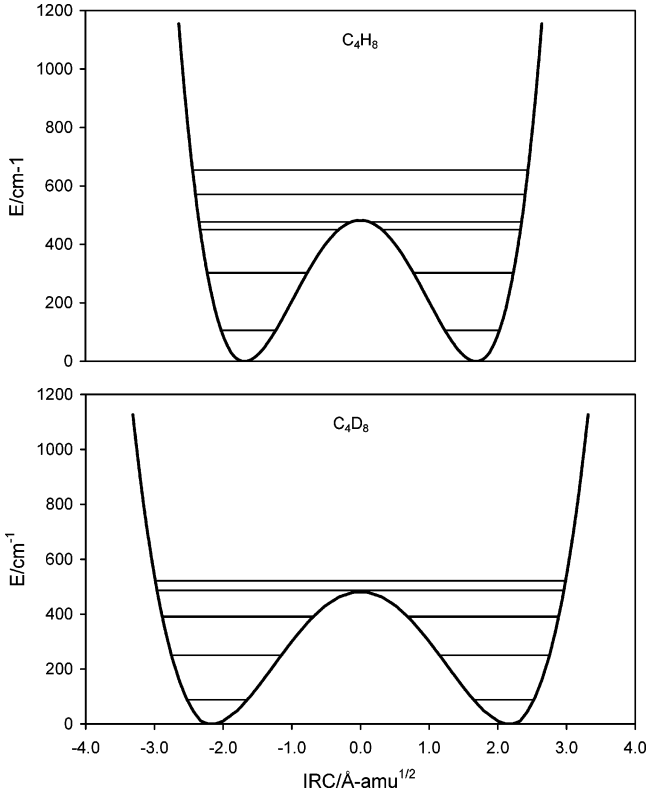

Figure 5. Ring-puckering IRC potentials for cyclobutane and cyclobutane-d_8. The potentials were obtained at the CCSD(T)/CBS//MP2/cc-pVTZ level. The first four pairs of $n^{\pm}$ eigenvalues are shown for each potential. Note that the two lowest pairs of eigenstates are overlapping.

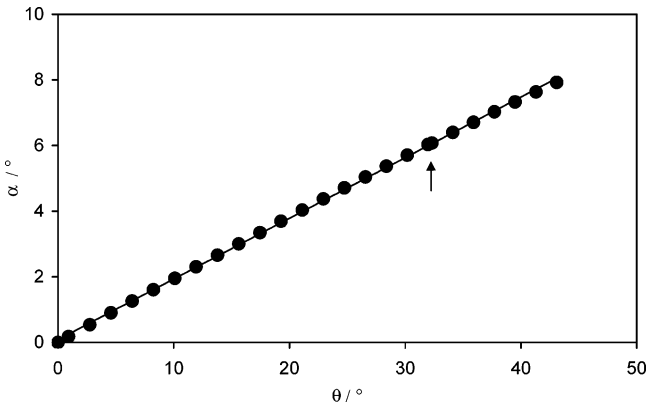

Figure 6. Plot of α vs θ along the IRC potential. The arrow indicates the equilibrium position.

Previous workers have fit the inversion potential to power series expressions, usually in terms of the variable z (see Figure 1). It is instructive to fit the IRC potential to a function of the form

$$V(z) = az^2 + bz^4 + cz^6 + d \qquad (2)$$

where d represents the barrier height. We obtained z values for geometries along the IRC, transformed V(IRC) to $V(z)$, and performed a regression analysis with respect to eq 2. Figure 7 portrays our calculated potential superimposed on that obtained by Egawa et al.[16] based on a fit of IR data to eq 2 in which δ was constrained to 0.22. Their value of the barrier height thus obtained, 510 cm^{-1}, is somewhat higher than our calculated value of 482 cm^{-1}. The values of z_{eq} are in very close agreement at 0.140 and 0.138 Å for the IRC and the experimentally fitted

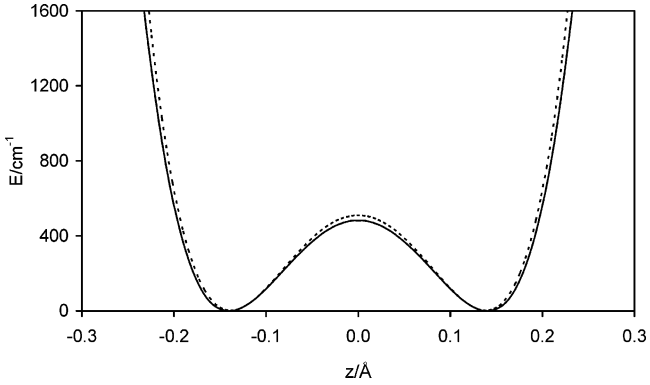

Figure 7. IRC potential (solid curve) for cyclobutane plotted vs z (cf Figure 1) and the potential assigned by Egawa et al.[16] (dashed curve, cf Table 2).

TABLE 2: Optimized Parameters Obtained from the Fits of eq 2 to the IRC Potential [CCSD(T)/CBS//MP2/cc-pVTZ] and to Experimental Data[a]

parameter	IRC	experiment[b]
a/10^4 cm^{-1} Å^{-2}	−4.92 (0.012)	−5.20 (0.06)
b/10^6 cm^{-1} Å^{-4}	1.22 (0.006)	1.28 (0.04)
c/10^6 cm^{-1} Å^{-6}	1.44 (0.078)	2.6 (0.6)
d/cm^{-1}	484 (0.5)	510 (2)

[a] IRC values are from the fit to the CCSD(T)/CBS//MP2/cc-pVTZ potential. Values in parentheses are standard deviations for the IRC fit and fitting errors for the experimental (IR) data, respectively. [b] Ref 16. Based on a fixed value of $\delta = 0.22$.

TABLE 3: Eigenvalues (in cm^{-1}) of the CCSD(T)/CBS//MP2/cc-pVTZ IRC Potentials for Cyclobutane and Cyclobutane-d_8

eigenstate	C_4H_8	C_4D_8
0^+	106.3085	88.0350
0^-	106.3203	88.0355
1^+	301.9016	249.9812
1^-	303.0959	250.0522
2^+	451.0239	389.4388
2^-	476.9842	392.9287
3^+	571.5756	486.2383
3^-	654.6371	521.5794
4^+	755.2377	590.9857
4^-	864.0434	661.3607
5^+	981.0809	740.3739
5^-	1105.4809	825.0765
6^+	1373.6506	915.1138
6^-	1516.5637	1009.8373

potentials, respectively. The corresponding values of θ_{eq} are 31.9 and 28.8°, respectively. Table 2 lists the optimized parameters obtained from fitting the ab initio potential to eq 2 along with those reported by Egawa et al.[16]

The one-dimensional IRC Hamiltonian was diagonalized using a finite difference method to obtain the inversion eigenvalues of cyclobutane and cyclobutane-d_8. We used these values to assess the ability of the potentials to predict the transition energies related to the Raman and IR spectra of these compounds. Because cyclobutane has no permanent dipole moment, inversion transitions can be directly observed only in Raman spectra and in combination bands with IR-allowed transitions. The double-minimum potential produces symmetric and antisymmetric eigenstates denoted by quantum numbers $n^{\pm}$. Because of the relatively low barrier of this potential (i.e., 480 cm^{-1}) and the relatively small separation of the minima, heavy atom tunneling is manifest by splittings in the + and − eigenstates of a given n value. Table 3 contains the eigenvalues

TABLE 4: Ring-Puckering Mode Transition Energies (in cm^{-1}) Obtained from IRC Potentials and from Experiment

	C_4H_8				$C4D_8$	
transition	IRC	Raman[a]	Raman[b]	IR[c]	IRC	Raman[b]
$0^{+-}1^{+}$	195.6				161.9	157.1
$0^{--}1^{-}$	196.2	197	199.4	198.6	162.0	
$1^{+-}2^{+}$	149.1	155	159.3		139.4	141.3
$1^{--}2^{-}$	173.9	175	177.1	174.9[d]	142.9	
$2^{+-}3^{+}$	120.6	117	119.2	117.4	96.8	105
$2^{--}3^{-}$	177.7		177.1	174.8	128.7	128.2
$3^{+-}4^{+}$	183.7			176.1[d]	104.7	92
$3^{--}4^{-}$	209.4			204.1	139.8	132.9
$4^{+-}5^{+}$	225.8			220.1	149.4	
$4^{--}5^{-}$	241.4			236.0	163.7	

[a] Ref 6. [b] Ref 8. [c] Ref 16. [d] Switched assignments in ref 19.

TABLE 5: Splittings (in cm^{-1}) of the $n^{\pm}$ Levels for Cyclobutane and Cyclobutane-d_8 Obtained from the IRC and Experimentally Based Potentials

	C_4H_8			C_4D_8		
n	IRC	Raman[a]	IR[b]	IRC	Raman[a]	IR[b]
0	0.012	0.01	0.01	0.001	0.0	0.0
1	1.2	0.83	0.76	0.007	0.03	0.04
2	26.0	20.2	19.4	3.5	1.6	1.7
3	83.1	77.1	76.8	35.5	23.7	23.9
4	108.8	105.5	105.8	70.4	63.2	63.2
5	124.4	120.9	128.3	84.7	79.7	79.7

[a] Ref 6. [b] Ref 16.

associated with the IRC potentials shown in Figure 5, which also depicts the eigenvalues up to $n^{\pm} = 4$.

The Raman and IR transitions predicted by the IRC potentials, along with the respective experimental data, are summarized in Table 4. The agreement is impressive, especially considering the uncertainties in the experimental frequencies and assignments and the fact that there are no adjustable parameters in the IRC-obtained values. Data for cyclobutane-d_8 are limited, but on the basis of the IRC results, it is reasonable to suggest that the assignments made by Miller and Capwell[8] for the $2^{+-}3^{+}$ and $3^{+-}4^{+}$ transitions (i.e., 105 and 92 cm^{-1}, respectively) be reversed.

Although the tunneling splitting has not been observed directly, many investigators have calculated the $n^{\pm}$ energy differences from analytical potentials obtained from fitting the Raman and/or IR data. In Table 5, we compare the level splittings derived from the IRC potential with values calculated from empirical potentials. The agreement is generally satisfactory, although we note the larger discrepancies for cyclobutane-d_8.

Origin of the Inversion Barrier

The conventional view of four-membered ring systems suggests that inversion barriers arise from the interplay of two electronic effects. Ring strain favors a planar structure since puckered geometries necessarily have bond angles slightly less than 90°, and thus, greater bond bending. Torsional strain involving the eclipsed C−H bonds of the planar structure is, however, reduced as the ring puckers. Evidently, the puckering motion more effectively diminishes torsional strain than it enhances ring strain; the equilibrium geometry of cyclobutane is, therefore, puckered. Ethane is the classic example of a hydrocarbon in which a barrier, in this case that of internal rotation, is traditionally associated with torsional strain. Recent work[39−43] has reemphasized the view that such barriers can better be understood as arising from hyperconjugative interactions. We performed NBO analysis of the Hartree−Fock (HF) wave function for each of the geometries along the IRC and explore here the influence of hyperconjugation on the inversion potential. We note that the C atoms remain essentially sp^3-hybridized (74.2−74.4% *p*-character in the C−C bonds) across the potential so that rehybridization likely has limited impact on ring puckering.

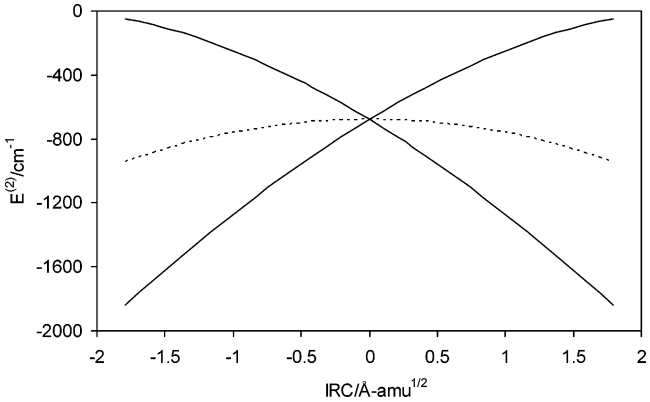

Figure 8. Second-order perturbation theory estimates of the $\sigma_{CC} \rightarrow \sigma_{CH}^*$ interaction strengths along the IRC. The solid curves represent the strengths of individual interactions, interactions with equatorial C−H antibonds for the lower portions of the curves and with axial antibonds for the upper portions. The dashed curve represents the average interaction strength.

The dominant hyperconjugative interactions in cyclobutane are those that delocalize a small portion of electron density from the C−C bonds (σ_{CC}) into vicinal C−H antibonds (σ_{CH}^*). Figure 8 shows the second-order perturbative estimates of the interaction strengths along the IRC. At the planar geometry (IRC = 0), each C−C bond interacts equally with four vicinal C−H antibonds. Thus, there are 16 equivalent $\sigma_{CC} \rightarrow \sigma_{CH}^*$ interactions in planar cyclobutane, each stabilizing this geometry by −680 cm^{-1}. D_{2d} distortion splits the interactions into two groups, eight involving delocalization into equatorial C−H antibonds and eight involving delocalization into axial. Distortion strengthens the interactions with the equatorial antibonds as the backside lobes of the carbon hybrids increasingly overlap the C−C bonds. In contrast, interactions with the axial antibonds are weakened as the corresponding overlap is diminished. In the equilibrium D_{2d} geometries, interactions with the equatorial antibonds have strengthened to 1840 cm^{-1}, whereas those with the axial antibonds have weakened to only 50 cm^{-1}. The dashed curve in Figure 8 represents the average strength of a $\sigma_{CC} \rightarrow \sigma_{CH}^*$ interaction along the IRC. The puckered geometries are more strongly stabilized (by approximately 260 cm^{-1} per interaction) than the planar form. Figure 9 is a stereoview of D_{2d} cyclobutane showing the interaction of a C−C bond with an equatorial C−H antibond. Note that the C−C bond is not symmetric about the line-of-centers. Rather, the orbital centroid is displaced to the outside of the ring, reflecting the strained nature of this orbital. The bond strongly overlaps the backside lobe of the C−H antibond within the ring region.

The cyclobutane wave functions also reveal significant hyperconjugative interactions between the C−H bonds and vicinal C−H antibonds, $\sigma_{CH} \rightarrow \sigma_{CH}^*$. Although somewhat weaker than the C−C bond delocalizations discussed previously, the $\sigma_{CH} \rightarrow \sigma_{CH}^*$ interactions likewise tend to stabilize the D_{2d} geometries. Each C−H bond delocalizes into four vicinal C−H antibonds, participating in two trans-type interactions and two cis-type. There is a total, therefore, of 32 $\sigma_{CH} \rightarrow \sigma_{CH}^*$ interactions in cyclobutane, 16 trans and 16 cis. Strengths of the trans interactions are shown in Figure 10. In planar

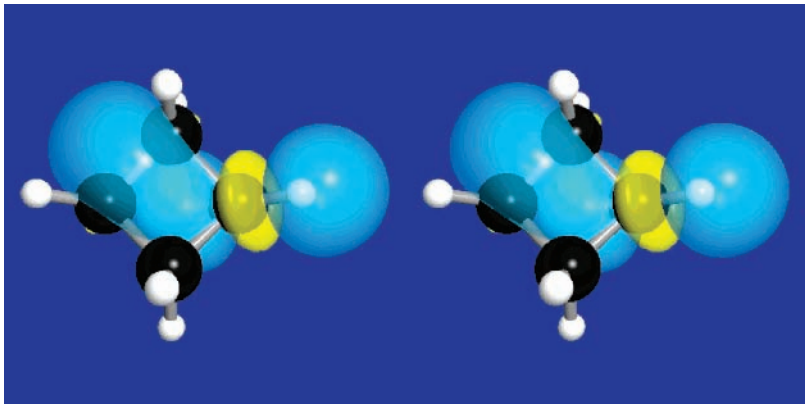

Figure 9. Stereoview of an equatorial $\sigma_{CC} \rightarrow \sigma_{CH}^*$ interaction in D_{2d} cyclobutane. The centroid of the strained C−C bond (between the upper left carbons) is somewhat shifted to the outside of the ring. The bond overlaps the backside lobe of the C−H antibond within the ring. The blue and yellow colors, respectively, represent the positive and negative phases of the orbitals.

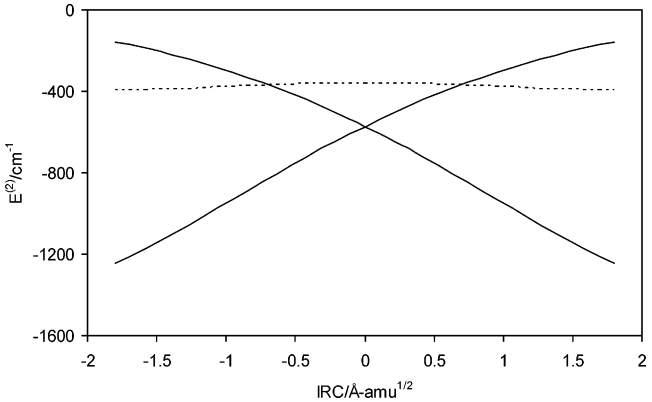

Figure 10. Second-order perturbation theory estimates of the trans-type $\sigma_{CH} \rightarrow \sigma_{CH}^*$ interaction strengths along the IRC. The solid curves represent the strengths of individual interactions, axial−axial for the lower portions of the curves and equatorial−equatorial for the upper portions. The dashed curve represents the average interaction strength, including both trans- and cis-type interactions.

cyclobutane, the trans interactions are fairly strongly stabilizing, at -575 cm^{-1}, while the cis interactions (not shown) are rather weak, at -150 cm^{-1}. The 16 trans interactions split into two groups (eight axial−axial and eight equatorial−equatorial) upon D_{2d} distortion. The more important of these are the axial−axial interactions that strengthen, due to increasing bond−antibond overlap, to -1240 cm^{-1} in the equilibrium geometries. Figure 11 is a stereoview of one of these interactions, the principal C−H bonding lobe overlapping strongly with the backside lobe of the vicinal C−H antibond. Equatorial−equatorial interactions weaken to -160 cm^{-1} in equilibrium cyclobutane. The dashed curve in Figure 10 represents the average stabilization of a $\sigma_{CH} \rightarrow \sigma_{CH}^*$ interaction in cyclobutane. These interactions stabilize the equilibrium cyclobutane structure slightly more strongly (by 35 cm^{-1} per interaction) than in the planar form.

The origin of the coupling of the ring-puckering and CH_2-rocking motions along the IRC potential can also be understood in terms of hyperconjugation. As the ring puckers, the CH_2 groups undergo rocking motions that strengthen the donor−acceptor interactions. The equatorial C−H antibonds pivot about the C atoms, enhancing the overlaps of their backside lobes with vicinal C−C bonds. Similarly, the axial C−H antibonds pivot to enhance their overlaps with vicinal C−H bonds. Thus, the puckering and rocking motions act in concert to stabilize the strained cyclobutane structure.

To more fully judge the influence of hyperconjugation on inversion, we examined the character of the ring-puckering potential at the HF level in the absence of $\sigma_{CC} \rightarrow \sigma_{CH}^*$ or $\sigma_{CH} \rightarrow \sigma_{CH}^*$ interactions. Calculations were performed using the energetic analysis of the NBO method, and results are shown in Figure 12. We chose the origin of the energy scale to correspond to the energy of planar cyclobutane for all calculations. The HF method yields the usual double minimum potential revealing two equilibrium D_{2d} structures separated by the planar D_{4h} transition state. The barrier is only 360 cm^{-1}, somewhat lower than the experimental and CCSD(T) estimates, but sufficiently large that these HF-level calculations should reveal the essential qualitative nature of the potential. Using the energetic analysis, we deleted the 16 $\sigma_{CC} \rightarrow \sigma_{CH}^*$ interactions

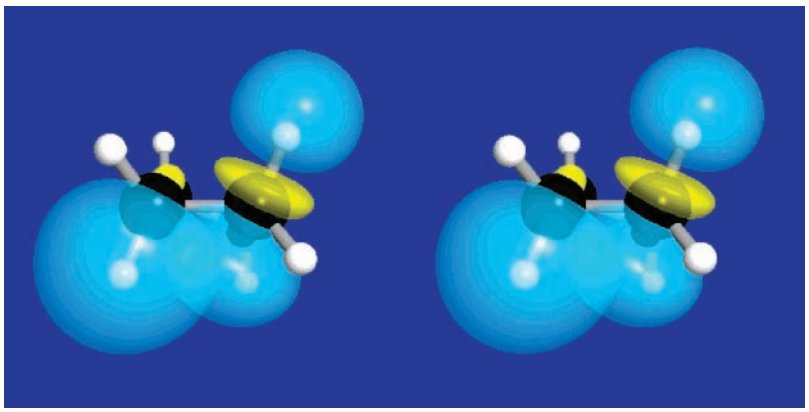

Figure 11. Stereoview of an axial−axial $\sigma_{CH} \rightarrow \sigma_{CH}^*$ interaction in D_{2d} cyclobutane. The bond of the left-hand carbon strongly overlaps with the backside lobe of the C−H antibond of the right-hand carbon. The blue and yellow colors, respectively, represent the positive and negative phases of the orbitals.

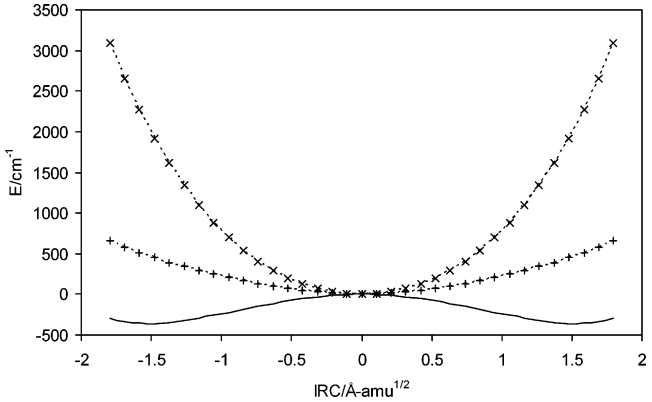

Figure 12. Inversion potentials for cyclobutane. The solid curve represents the HF energy of cyclobutane along the IRC, revealing the expected double-minimum potential. The dashed curves are the inversion potentials for cyclobutane after deleting either the $\sigma_{CC} \rightarrow \sigma_{CH}^*$ (crosses) or the $\sigma_{CH} \rightarrow \sigma_{CH}^*$ (pluses) interactions. For clarity, the energy of planar cyclobutane is arbitrarily set of zero for each potential.

and reevaluated the energy of each of the geometries along the IRC. These calculations yield a single minimum potential (the crosses in Figure 12) with a planar equilibrium geometry. Similarly, we performed a separate series of calculations in which the 32 $\sigma_{CH} \rightarrow \sigma_{CH}^*$ interactions were deleted. The resulting potential (the pluses in Figure 12) also exhibits a single minimum at the planar geometry. These results clearly demonstrate that hyperconjugative interactions (indeed, principally the equatorial $\sigma_{CC} \rightarrow \sigma_{CH}^*$ and axial−axial $\sigma_{CH} \rightarrow \sigma_{CH}^*$ interactions) favorably stabilize the puckered geometries relative to the planar form. The stronger delocalizing interactions of puckered cyclobutane can be viewed as the origin of the inversion barrier.

Summary

Ring-puckering and CH_2-rocking angles in cyclobutane, which have eluded definitive characterization experimentally, have been obtained from high-level ab initio calculations. Our best estimates of these quantities, obtained at the CCSD(T)/cc-pVQZ level, are 29.59 and 5.67°, respectively, corresponding to a coupling between puckering and rocking motions of $\delta = 0.192$. The calculated angles are within the range of experimental results. Our best estimate of the inversion barrier, 482 cm^{-1}, determined from CCSD(T)/CBS//CCSD(T)/cc-pVQZ calculations, is also consistent with values determined from spectroscopic studies.

IRC potentials, which are free of adjustable parameters, capture reasonably well the energetics of inversion in cyclobutane and cyclobutane-d_8, and thus, are able to account for the coupling between ring puckering and CH_2 rocking. Values of δ along the IRC deviate marginally from the equilibrium value and support the semirigid bender model that has been used to describe the ring inversion in cyclobutane. The IRC potentials also account well for the assigned ring-puckering transitions observed in IR and Raman spectra of cyclobutane and its d_8 isotopomer.

We also examined the origin of the inversion barrier in cyclobutane. Analysis of cyclobutane wave functions along the IRC pathway identified the important role of hyperconjugation. Equatorial $\sigma_{CC} \rightarrow \sigma_{CH}^*$ and axial−axial $\sigma_{CH} \rightarrow \sigma_{CH}^*$ donor−acceptor interactions strengthen upon ring puckering and CH_2 rocking, thereby acting to stabilize the puckered D_{2d} geometries relative to the planar D_{4h} form. Analysis of cyclobutane along the IRC reveals that the puckering potential assumes a single minimum form, with a stable D_{4h} geometry, in the absence of these hyperconjugative interactions.

References and Notes

(1) Rathjens, G. W., Jr.; Gwinn, W. D. *J. Am. Chem. Soc*. **1953**, *75*, 5629−5633.
(2) Rathjens, G. W., Jr.; Freeman, N. K.; Gwinn, W. D.; Pitzer, K. S. *J. Am. Chem. Soc*. **1953**, *75*, 5634−5642.
(3) Ueda, T.; Shimanouchi, T. *J. Chem. Phys.* **1968**, *49*, 470−471.
(4) Wright, J. S.; Salem, L. *J. Chem. Soc. Chem. Commun.* **1969**, 1370−1371.
(5) Wright, J. S.; Salem, L. *J. Am. Chem. Soc.* **1971**, *93*, 2−329.
(6) Stone, J. M. R.; Mills, I. M. *Mol. Phys.* **1970**, *18*, 631−652.
(7) Meiboom, S.; Snyder, L. C. *J. Chem. Phys.* **1970**, *52*, 3857−3863.
(8) Miller, F. A.; Capwell, R. J. *Spectrochim. Acta* **1970**, *27A*, 947−956.
(9) Pasternak, R.; Amyer, A. Y. *J. Mol. Struct.* **1972**, *13*, 201−210.
(10) Malloy, T. B., Jr.; Lafferty, W. J. *J. Mol. Spectrosc.* **1975**, *54*, 20−38.
(11) Combs, L. L.; Holloman, M. *J. Mol. Struct.* **1976**, *33*, 289−305.
(12) Bauld, N. L.; Cessac, J.; Holloway, R. L. *J. Am. Chem. Soc*. **1977**, *99*, 8140−8144.
(13) Cremer, D. *J. Am. Chem. Soc.* **1977**, *99*, 1307−1309.
(14) Cremer, D.; Dorofeeva, O. V.; Mastryokov, V. S. *J. Mol. Struct.* **1980**, *62*, 259−273.
(15) Rafilipomanana, C.; Cavagnat, D.; Cavagnat, R.; Lassegues, J. C. *J. Mol. Struct.* **1985**. *127*, 283−296.
(16) Egawa, T.; Fukuyama, T.; Yamamoto, S.; Takabayashi, F.; Kambara, H.; Ueda, T.; Kuchitsu, K. *J. Chem. Phys.* **1987**, *86*, 6018−6026.
(17) Egawa, T.; Yamamoto, S.; Kuchitsu, K. *J. Mol. Spectrosc.* **1988**, *129*, 72−85.
(18) Vogelsanger, B.; Caminati, W.; Bauder, A. *Chem. Phys. Lett.* **1987**, *141*, 245−250.
(19) Caminati, W.; Vogelsanger, B.; Meyer, R.; Grassi, G.; Bauder, A. *J. Mol. Spectrosc.* **1988**, *131*, 172−184.
(20) Egawa, T.; Yamamoto, S.; Ueda, T.; Kuchitsu, K. *J. Mol Spectrosc.* **1987**, *126*, 231−239.
(21) Laane, J. *J. Phys. Chem.* **1991**, *95*, 9246−9249.
(22) Stein, A.; Lehmann, C. W.; Luger, P. *J. Am. Chem. Soc.* **1992**, *114*, 7684−7687.
(23) Champion, R.; Godfrey, P. D.; Bettens, F. L. *J. Mol. Spectrosc*. **1992**, *155*, 18−24.
(24) Durig, J. R.; Zhao, W. *J. Phys. Chem.* **1994**, *98*, 9202−9206.
(25) Fukui, K. *J. Phys. Chem.* **1970**, *74*, 4161−4163.
(26) Fukui, K. *Acc. Chem. Res.* **1981**, *14*, 363−368.
(27) Reed, A. E.; Weinhold, F. *Chem. Rev.* **1988**, *88*, 899−926.
(28) *NBO 5.0*; Glendening, E. D.; Badenhoop, J. K.; Reed, A. E.; Carpenter, J. E.; Bohmann, J. A.; Morales, C. M.; Weinhold, F. Theoretical Chemistry Institute, University of Wisconsin: Madison, WI, 2001.
(29) Becke, A. D. *J. Chem. Phys.* **1993**, *98*, 5648−5652.
(30) Frisch, M. J.; Head-Gordon, M.; Pople, J. A. *Chem. Phys. Lett.* **1990**, *166*, 281−289 and references therein.
(31) Hampel, C.; Peterson, K.; Werner, H.-J. *Chem. Phys. Lett.* **1992**, *190*, 1−12 and references therein.
(32) Dunning, T. H., Jr. *J. Chem. Phys.* **1989**, *90*, 1007−1023.
(33) *GAMESS version 6 (R5)*; Schmidt, M. W.; Baldridge, K. K.; Boatz, J. A.; Elbert, S. T.; Gordon, M. S.; Jensen, J. H.; Koseki, S.; Matsunaga, N.; Nguyen, K. A.; Su, S. J.; Windus, T. L.; Dupuis, M.; Montgomery, J. A. *J. Comput. Chem.* **1993**, *14*, 1347−1363.
(34) MOLPRO is a package of ab initio programs written by Werner, H.-J.; Knowles, P. J. with contributions from Amlöf, J.; Amos, R. D.; Berning, A.; Cooper, D. L.; Deegan, M. J. O.; Dobbyn, A. J.; Eckert, F.; Elbert, S. T.; Hampel, C.; Lindh, R.; Lloyd, A. W.; Meyer, W.; Nicklass, A.; Peterson, K.; Pitzer, R.; Stone, A. J.; Taylor, P. R.; Mura, M. E.; Pulay, P.; Schütz, M.; Stoll, H.; Thorsteinsson, T.
(35) Frisch, M. J.; Trucks, G. W.; Schlegel, H. B.; Scuseria, G. E.; Robb, M. A.; Cheeseman, J. R.; Zakrzewski, V. G.; Montgomery, J. A., Jr.; Stratmann, R. E.; Burant, J. C.; Dapprich, S.; Millam, J. M.; Daniels, A. D.; Kudin, K. N.; Strain, M. C.; Farkas, O.; Tomasi, J.; Barone, V.; Cossi, M.; Cammi, R.; Mennucci, B.; Pomelli, C.; Adamo, C.; Clifford, S.; Ochterski, J.; Petersson, G. A.; Ayala, P. Y.; Cui, Q.; Morokuma, K.; Malick, D. K.; Rabuck, A. D.; Raghavachari, K.; Foresman, J. B.; Cioslowski, J.; Ortiz, J. V.; Baboul, A. G.;. Stefanov, B. B.; Liu, G.; Liashenko, A.; Piskorz, P.; Komaromi, I.; Gomperts, R.; Martin, R. L.; Fox, D. J.; Keith, T.;. Al-Laham, M. A.; Peng, C. Y.; Nanayakkara, A.; Gonzalez, C.; Challacombe, M.; Gill, P. M. W.; Johnson, B.; Chen, W.; Wong, M. W.; Andres, J. L.; Head-Gordon, M.; Replogle, E. S.; Pople, J. A. *Gaussian 98*, revision A.7; Gaussian, Inc.: Pittsburgh, PA, 1998.
(36) Gonzalez, C.; Schlegel, H. B. *J. Chem. Phys.* **1989**, *90*, 2154−2161.

(37) Peterson, K. A.; Woon, D. E.; Dunning, T. H., Jr. *J. Chem. Phys.* **1994**, *100*, 7410−7415.
(38) Woon, D. E.; Dunning, T. H., Jr. *J. Chem. Phys.* **1994**, *101*, 8877−8893.
(39) Reed, A. E.; Weinhold, F. *Israel J. Chem.* **1991**, *31*, 277−285.
(40) Goodman, L.; Gu, H. B. *J. Chem. Phys.* **1998**, *109*, 72−78.
(41) Goodman, L.; Gu, H. B.; Pophristic, V. *J. Chem. Phys.* **1999**, *110*, 4268−4275.
(42) Goodman, L.; Pophristic, V.; Weinhold, F. *J. Am. Chem. Soc.* **1910**, *32*, 983−993.
(43) Badenhoop, J. K.; Weinhold, F. *Int. J. Quantum Chem.* **1999**, *72*, 269−280.